

Title:

PARP1 Suppresses the Transcription of PD-L1 by Poly(ADP-Ribosyl)ating STAT3

Running title: PARP1 Suppresses the Transcription of PD-L1

Ling Ding^{1,#}, Xi Chen^{1,#}, Xiaqing Xu¹, Yuli Qian², Guikai Liang¹, Fengqi Yao¹, Zhangting Yao¹, Honghai Wu¹, Jieqiong Zhang¹, Qiaojun He^{1,*}, and Bo Yang^{1,*}

¹Author's Affiliations: Zhejiang Province Key Laboratory of Anti-Cancer Drug Research, Institute of Pharmacology and Toxicology, College of Pharmaceutical Sciences, Zhejiang University, Hangzhou, China, 310058

²Department of Reproductive Endocrinology, Women's Hospital, School of Medicine, Zhejiang University, Hangzhou, China, 310006

[#]Co-first author: These authors contributed equally to this work

^{*}Corresponding Author: Bo Yang, Room 427, Institute of Pharmacology and Toxicology, College of Pharmaceutical Sciences, Zhejiang University, Hangzhou, China, 310058, E-mail: yang924@zju.edu.cn. Phone/Fax: +86-571-88208400; and Qiaojun He, Room 113, Institute of Pharmacology and Toxicology, College of Pharmaceutical Sciences, Zhejiang University, Hangzhou, China, 310058, E-mail: qiaojunhe@zju.edu.cn. Phone/Fax: +86-571-88208400.

Disclosure of Potential Conflicts of Interest: No potential conflicts of interest were disclosed.

Funding: This work was supported by National Natural Science Foundation of China (for Distinguished Young Scholar, No. 81625024 to Yang B.); National Natural Science Foundation of China (No. 81773754 and No.81573428 to Ding L.).

Keywords: PARP1, PD-L1, RARylation, STAT3, phosphorylation

Counts: Abstract 211; Text 4826; 7 Figures; 7 Supplementary Figures; 3 Supplementary Tables

Abstract

Studies have pointed to a role of PARP1 in regulating gene expression through poly(ADP-ribosyl)ating, sequence-specific, DNA-binding transcription factors. However, few examples exist that link this role of PARP1 to the immunogenicity of cancer cells. Here, we report that PARP1 poly(ADP-ribosyl)ates STAT3 and subsequently promotes STAT3 de-phosphorylation, resulting in reduced transcriptional activity of STAT3 and expression of PD-L1. In this study, we showed that PARP1 silencing or pharmacological inhibition enhanced the transcription of PD-L1 in cancer cells, which was accompanied by the upregulation of PD-L1 protein expression, both in the cytoplasm and on the cell surface. This induction of PD-L1 was attenuated in the absence of the transcription factor STAT3. Cell-based studies indicated that PARP1 interacted directly with STAT3 and caused STAT3 poly(ADP-ribosyl)ation. STAT3's activation of PD-L1 transcription was abolished by the over-expression of wild-type PARP1 but not mutant PARP1, which lacks catalytic activity. PARP1 downregulation or catalytic inhibition enhanced the phosphorylation of STAT3, which was reversed by the ectopic expression of wild-type PARP1 but not by mutated PARP1. An inverse correlation between PARP1 and PD-L1 was also observed in clinical ovarian cancer samples. Overall, our study revealed PARP1-mediated poly(ADP-ribosyl)ation of STAT3 as a key step in inhibiting the transcription of PD-L1, and this mechanism exists in a variety of cancer cells.

Introduction

Poly (ADP-ribose) polymerases (PARPs) are enzymes that transfer ADP-ribose groups to target proteins, thereby affecting various nuclear and cytoplasmic processes (1). PARP1, the founding member of the PARP family, was characterized for a long time as a DNA damage sensor and a key factor in DNA repair systems. However, it has become increasingly clear that PARP1 also plays an important role in gene expression through the poly(ADP-ribosyl)ation (PARylation) of sequence-specific DNA-binding transcription factors (2). For example, PARP1 can poly(ADP-ribosyl)ate NELF (negative elongation

factor) and promote its release from paused RNA polymerase II, allowing productive elongation and RNA production (3). By poly(ADP-ribosyl)ating Smad3 and Smad4, PARP1 dissociates Smad complexes from DNA, which can attenuate Smad-specific gene expression (4). PARP1 can also ADP-ribosylate the regulatory T cell (Treg)-specific transcription factor FOXP3, which subsequently promotes its degradation and, therefore, negatively regulates Treg function (5). C/EBP β , an adipogenic transcription factor, is reported to be ADP-ribosylated by PARP1, resulting in the inhibition of its DNA-binding activity and the subsequent arrest of the adipogenic transcriptional program (6). These findings directly link PARylation to biological outcomes, including cell differentiation, the post-transcriptional regulation of RNA, and metabolic functions. Although PARP1 has been shown to play a critical role in gene regulation, very limited substrates have been identified because of the labile nature of the ADP-ribose linkage to the protein, the dynamic nature of the modification, the heterogeneity in its signal, and its rarity (7).

Over the last few years, there have been major breakthroughs in our understanding of tumor-associated immune suppression. Among the multiple mechanisms that can contribute to immune suppression in the tumor microenvironment, programmed death ligand 1 (PD-L1), an inhibitory member of the B7 family, plays a central role in the evasion of the immune system by many cancer types (8,9). PD-L1 expression is upregulated in various epithelial tumors, including ovarian cancer (10), breast cancer (11), non-small cell lung carcinoma (12), and the colon cancer (13). PD-L1 binds to either PD-1 or CD80 receptors on T cells, B cells, dendritic cells, and natural killer cells to inhibit their proliferation, cytokine release, and cytolytic activity, whereas the blockade of co-inhibitory ligation with monoclonal antibodies, such as PD-L1 or PD-1 antibodies, restores T-cell function and increases therapeutic efficacy (14). The impressive and durable clinical response of PD-L1 or PD-1 blockade immunotherapy led to the FDA approval of nivolumab, pembrolizumab, and atezolizumab for the treatment of multiple types of cancer (15-17).

The expression of PD-L1 is commonly elevated in cancer cells and is an important mechanism that negatively regulates T-cell activation to prevent autoimmune responses under physiological conditions (14). Studies have also focused on how and when PD-L1 is upregulated during the pathogenesis of cancer, and several transcriptional factors have been shown to be involved in the expression of PD-L1 (18). HIF-1 α regulates PD-L1 by binding to a hypoxia response element (HRE) in the PD-L1 promoter to activate PD-L1 transcription (19). STAT3 has also been demonstrated to bind to the PD-L1 promoter to transcriptionally regulate its expression (20). PD-L1 is commonly expressed and transcriptionally can be regulated by STAT3 and MYC in ALK-negative anaplastic large cell lymphoma (21). NF- κ B is involved in LMP1-induced PD-L1 expression and is also a major mediator of INF γ -induced PD-L1 expression(22). MYC regulates the expression of PD-L1 by binding to its promoter in murine and human leukemia and lymphomas (23). Although the transcriptional regulation of PD-L1 via NF- κ B, STAT, or MYC has been studied, the molecular mechanism controlling the transcriptional activity is still poorly understood.

In this study, we introduce PARP1 as a negative regulator of the STAT3-mediated transcription of PD-L1 in various cancers. We showed that PARP1 poly(ADP-ribosyl)ated STAT3, inhibited its phosphorylation and transcriptional activities, and attenuated the expression of PD-L1. Our results provide a clear example of PARP1-regulated gene expression, uncover a post-translational modification of STAT3, and improve the understanding of the mechanism that regulates the expression of PD-L1.

Methods

Antibodies and Reagents

The antibodies against PD-L1 (#sc-50298), PARP1 (#sc-7150), STAT3 (#sc-482X), STAT3 (#sc-482), anti-rabbit IgG (#sc-2007), HA (#sc-7392), Actin (#sc-1615), STAT1 (#sc-346), MYC (#sc-56634), and Protein A/G (#sc-2003) were purchased from Santa Cruz Biotechnology (Dallas, Texas, USA). Anti-PAR (#4335-AMC-050) was purchased

from Trevigen (Gaithersburg, MD, USA). PE-conjugated phospho(p)-STAT3 (Tyr705) (DA37) rabbit monoclonal antibody (mAb; #8119), STAT3 (#4904S), p-STAT3 (#9145L), GSK3 β (#12456), PD-L1 (#13684S), and p-GSK3 β (#5558S) were purchased from Cell Signaling Technology (Danvers, MA, USA). Anti-DYKDDDDK-tag (#A00187) and anti-DYKDDDDK IP resin (#L00425) were purchased from GenScript (Piscataway, NJ, USA). The anti-HA affinity gel (#B23302) was purchased from BioTools (Houston, TX, USA). The siRNA-negative control and sequence-specific short RNA duplex pools for interference were purchased from GenePharma (Suzhou, China). The PARP inhibitors olaparib (#S1060), veliparib (#S1004), talazoparib (#S7048), A-966492 (#S2197), vanadate (#S2000), and AZD1480 (#S2162) were obtained from Selleck (Houston, TX, USA). The propidium iodide (#ZF-50-0001) was purchased from MultiSciences (Hangzhou, China). FITC-conjugated CD47 (#556045), FITC-conjugated CD274 (#558065), and FITC mouse IgG were purchased from BD Biosciences (San Jose, CA, USA). Sulforhodamine B (#230162) was purchased from Sigma-Aldrich (Burlington, MA, USA).

Cell Culture

All the cell lines were obtained from Cell Bank of Shanghai Institutes for Biological Sciences, Chinese Academy of Sciences (March 2013 and September 2016). Each new aliquot was passaged in our laboratory for fewer than three months after resuscitation, after which new seed stocks were thawed. All the cell lines were authenticated using DNA fingerprinting (variable number of tandem repeats), confirming that no cross contamination occurred during this study. Cell lines were tested for mycoplasma contamination at least every month when they were in use (SKOV3 and OVCAR8 were latest tested on 3rd July 2018 and other cell lines were latest tested on 9th September 2017). SKOV3, OVCAR8, PC9, and SW620 were maintained in RPMI-1640 (Gibco, #31800, USA) with 10% fetal bovine serum (FBS), (ExCellBio, #FSP500, China). HEK293T was cultured in DMEM (Gibco, #12800, USA) with 10% FBS (Gemini, #900-108,

USA). A549 was maintained in F12 (Sigma, #N670, USA) and 10% FBS (Gemini). Colo205 was maintained in DMEM (Gibco) and 10% FBS (ExCellBio). All the media contained 1% penicillin/streptomycin (Gibco, #15140122, USA), and all cells were maintained at 37°C in a 5% CO₂ incubator.

Plasmid Construction and Transfection

The mammalian expression vector PCMV6 (#PS100001) and the full-length of PARP1 (#RC207085) and STAT3 (#NM 139276) were all purchased from Origene. The mutation of PARP1 was performed by site-directed mutagenesis and verified by sequencing. A mutation-specific PCR amplification method was developed as follows: 100 ng/μL full-length PARP1 or STAT3: 1μL; 10XPCR Buffer: 5 μL; 25 mM MgSO₄: 3 μL; 2 mM dNTPs: 5 μL; primers: 2 μL; KOD-Plus-Neo: 1 μL; double distilled water: 33 μL. All reagents used above contained in the KOD-Plus-Neo kit (#KOD-401) from Toyobo (Japan). The specific primers are detailed in Supplementary Table S1. HEK 293 Cells were transfected with the indicated plasmids using JetPRIME (Polyplus, #114-15) for indicated time, according to the manufacturer's instructions.

siRNA-Mediated Silencing

1.5X10⁵ SKOV3 or OVCAR8 cells were seeded in six well plate for each well and allowed to grow for 12 hours. Then cells were transfected with transfection reagent JetPRIME (Polyplus, #114-15) and STAT3 (PARP1, MYC, STAT1) siRNA or scrambled siRNA (siRNA-negative control, NC), JetPRIME Buffer (Polyplus, #712-60): 200 μL, jetprimer : 2 μL, 20 μM siRNA : 2.5 μL for each well) for 24 hours or 48 hours. The siRNA sequences are shown in Supplementary Table S2.

RNA Isolation and Quantitative Real-Time PCR

1.5X10⁵ SKOV3 or OVCAR8 cells were seeded in six well plate for each well and allowed to grow for 12 hours. Then cells were treated for 0 hour, 2 hours, 4 hours, 8 hours, 12 hours, or 24 hours with PARP inhibitors (10 μM Olaparib, 10 μM Veliparib, or 10 μM

A966492) or with DMSO alone (Con). For another study, cells were transfected with siRNA for 24 hours then treated with PARP inhibitors for another 12 hours or 24 hours. Total mRNA was collected by using Trizol Reagent (Invitrogen, #15596026), and RNA purity (A260/280 ratio of 2.0-2.1) and quantity was evaluated using the NanoDrop ND-1000 Spectrophotometer (Thermo Fisher Scientific). First-strand cDNA was synthesized from 2 µg of total RNA using TransScript One-Step gDNA Removal and cDNA Synthesis SuperMix (TRAN, #AT311-03). Quantitative RT-PCR was performed on 7500 Fast Dx Real-Time PCR Instrument (Applied Biosystems, Singapore). The reaction system (20 µL) was as follows: 2.5 µL forward and reverse primers (10 µM), 0.1 µg cDNA obtained from reverse transcription, respectively, 10 µL iTaq™ Universal SYBR Green Supermix (BioRad, #172-5124, USA), and DEPC water (Sangon Biotech, #B501005-0500, China) to 20 µL. The PCR protocol consisted of thermal cycling was as follows: Initial denaturation at 95 °C for 3 minutes, followed by 40 cycles at 95 °C (3 seconds) and 60 °C (31 seconds). To ensure that the targeted amplicon was amplified only, after the last extension step, melting curves were then generated and the temperature was increased from 60 to 95 °C at 0.1 °C/s. Fold changes in the expression of each gene were calculated using the formula $2^{-(\Delta\Delta Ct)}$ by a comparative threshold cycle (Ct) method. All reactions were performed in triplicate and beta-actin was used as the normalizing gene. The primers used are listed in Supplementary Table S3.

Heatmap

OVCAR8 cells were transfected with siRNA targeting PARP1 for 48 hours, and a series of immunosuppressive factors were analyzed by qRT-PCR, including genes for PD-L1, IL10, IL13, CXCL8, MIF, NOS2, COX2, B7H3, IDO, CD47, TIGIT, and CSF2. Heatmap representation of the fold change of 12 immunosuppressive factor mRNAs that were affected by PARP1 depletion was generated. Red represents increased expression while blue represents reduced expression. The z-score is specified on the left. The heatmap was created using Microsoft Excel 2013 (Microsoft Corporation, Seattle, USA) conditional formatting feature.

ChIP Assay

A ChIP assay was performed using the EZ ChIP™ chromatin immunoprecipitation kit (Millipore, # 17-371) according to the manufacturer's protocol. Briefly, SKOV3 cells were cross-linked by 1% (v/v) methanol-free formaldehyde (#252549, sigma, USA) for 10 minutes and then quenched using 125 mM glycine (#G6201, sigma, USA). Cells were collected in lysis buffer (contained in the CHIP™ kit) and were sonicated for 10 minutes in High mood into 200-500 bp fragments using Bioruptor plus (Diagenode, Belgium). Soluble chromatin-containing lysates obtained from aldehyde-fixed and sonicated SKOV3 cells were incubated with the STAT3 (#sc-482x) antibody, and rotated at 4°C overnight. Non-immunoprecipitated lysates (input) and immunoprecipitates obtained with the anti-rabbit IgG (Santa, #sc-2007) served as a positive and negative control, respectively. Next, the DNA-protein immune-complexes were precipitated with protein A-agarose beads (contained in the CHIP™ kit), and the DNA was then extracted with phenol/chloroform, precipitated with ethanol, and PCR-amplified using primers specific for the PD-L1 gene promoter: 5'-CAAGGTGCGTTCAGATGTTG-3' and 5'-GGCGTTGGACTTTCCTGA-3'. PCR was performed on Mastercycler nexus gradient PCR instrument (Eppendorf, USA). The reaction system (10 µL) was as follows: 2.0 µL DNA, 13.2 double distilled water, 2.0 µL 10XPCR Buffer, 1.6 µL 2.5 mM dNTP, 0.8 µL Primers, 0.4 µL Taq (5 U/µL), and the following PCR reaction program was used: Initial denaturation at 94 °C (3 minutes), followed by 32 cycles at 94 °C (20 seconds), 59 °C (30 seconds), 72 °C (2 minutes), and final extension at 72 °C (2 minutes). 10 µL of each PCR reaction was removed for analysis by 4% agarose (BioFroxx, #110GR100, Germany) gel electrophoresis.

Immunoprecipitation and Western Blot Analysis

The HEK293T cells were lysed in lysis buffer containing 25 mM Tris-base (pH 7.4), 1% NP-40, 150 mM NaCl, 1 mM PMSF, 1 mM Na₃VO₄, and leupeptin (5 µg/mL; Biosharp, BS140A, China). We employed the BCA protein assay to quantitate protein using BCA kit

(Yeasen, #20201, China), and then 500 µg of cell protein from supernatants were immunoprecipitated with anti-HA affinity gel or anti-DYKDDDDK IP resin for 12 hours at 4°C, followed by incubation for another 1 hour after mixing with 30 µL of protein A/G beads (Santa, #sc-2003). The whole immunocomplexes were then analyzed by Western blot. Briefly, the proteins were separated by ExpressPlus™ PAGE Gel (GenScript, #M42015C, USA), transferred to PVDF membranes (Immobilon, #IPVH00010), blocked in TBST (150 mM NaCl, 10 mM Tris-HCl, pH 7.5, and 0.1% Tween 20) containing 5% bovine serum albumin (Amersco, #0332) for 1 hour, and incubated with the STAT3 (santa, #sc-482) or PARP1 (santa, #sc-7150) antibodies at a dilution of 1:1000, then treated with anti-rabbit (Fdbio science, #FDR007, China) secondary antibodies at a dilution of 1:5000. The specific bands were analyzed by a Western blot infrared imaging system (Amersham Imager 600, #66210336).

Cellular PARylation Assays

HEK 293 cells transfected with HA-STAT3 and Flag-PARP1 were lysed in 4% SDS buffer (pH 8.0, 4% SDS, 150 mM NaCl, 50 mM triethylamine), followed by sonication at an output power of 500 W at 4 °C for three 5-second pulses. Because the 4% SDS can prevent PARylated proteins from binding to antibodies against PAR during the IP procedure, the lysates were diluted 1:9 with 1% NP-40 lysis buffer (pH 7.4, 25 mM Tris-base, 150 mM NaCl, 10% glycerol) after sonication. The diluted lysates (input) were immunoprecipitated by incubating with anti-HA affinity gel or anti-PAR. After an overnight incubation, the immunocomplexes incubated with anti-PAR were collected following incubation with 30 µL Protein A/G before extensive washing, or the anti-HA affinity gel was washed with wash buffer (pH 7.4, 25 mM Tris-base, 150 mM NaCl), and the immunoprecipitated proteins were analyzed by Western blot with the anti-PAR or anti-HA at a dilution of 1:1000. To normalize for input protein, 3-4% of each cell lysate was subjected to Western blot and probed with anti-HA (Diagbio, #db2603, China) and Anti-DYKDDDDK-tag (GenScript, #A00187), following the protocol described above.

Immunofluorescence Microscopy

For immunostaining, 10000 SKOV3 cells were fixed with 4% paraformaldehyde at room temperature for 20 minutes. The fixed cells were then rinsed with ice cold 1XPBS and permeabilized with 200 μ L PBS-T solution (0.1% Triton X-100 (BioFroxx, #2424) in PBS solution) at 4 °C for 10 minutes. The cells were rinsed with PBS for 5 minutes and blocked for non-specific interaction with 4% BSA in PBS solution at 37 °C for 30 minutes. After blocking, the cells were incubated with the p-STAT3 antibody (1:100) overnight at 4 °C. Secondary antibodies (1:200) used were green anti-rabbit (Invitrogen, #A-11008). The nuclei were counterstained with DAPI (Invitrogen, #D1306). The slides were imaged using an Olympus Fluoview-microscope (FV10i-O).

Luciferase Reporter Assays

A section corresponding to the PD-L1 promoter (-281 to +43 base pair [bp] relative to the transcription start site) were obtained by polymerase chain reaction (PCR) from SKOV3 genomic DNA by Genomic DNA Kit (Invitrogen, #K182001, USA). The construct was confirmed by DNA sequencing. The pGL4.14-PD-L1 plasmid was generated by inserting a KpnI/XhoI (KpnI, Biolab, #R3142S; XhoI, Takara, #1094A) fragment containing PD-L1 constructs into the KpnI-XhoI restriction site of the pGL4.14 vector (Promega, #E669A) as reported (24). Reporter activities were assayed using the dual luciferase/renilla assay system. The Renilla-luciferase-expressing plasmid (Promega, #E2231) was used as the internal control to normalize the transfection efficiency. The cells were collected 36 hours after co-transfected with PGL4.14-PD-L1, Renilla, Flag-PARP1, and HA-STAT3 using JetPRIME (PolyPlus, #114-15). The luciferase activity was detected using the Dual-Luciferase Reporter Assay System (Promega, #E1910) following the manufacturer's protocol. The results are expressed as relative luciferase activity (firefly luciferase/renilla luciferase).

Flow Cytometry

At the experimental end point, 4×10^5 SKOV3 and OVCAR8 cells were fixed with 4% formaldehyde for 15 minutes at 37°C and permeabilized on ice for 30 minutes in 90% methanol. After washing with PBS, the cells were then stained with PE-conjugated p-STAT3 and FITC-conjugated CD274, and incubated for 2 hours at room temperature. After washing with PBS, cells were resuspended in 0.5 mL of PBS to measure the expression of PD-L1 and p-STAT3 by BD FACSuite™ flow cytometry (BD bioscience). SKOV3 and OVCAR8 were harvested, washed twice with PBS, and blocked with 3% BSA at 37°C for 45 minutes. The cells were then stained with FITC-conjugated CD274 at 37°C for 2 hours ($5 \mu\text{L}/2 \times 10^5$ cells in 100 μL 0.2% BSA). The instrument threshold was kept constant throughout the detection by BD FACSuite™ (BD bioscience). 10^5 cells were analyzed for each sample.

Cell Viability and Apoptosis Assay

Cell viability was analyzed by sulforhodamine B staining as previously performed (25). Apoptosis was detected using propidium iodide (PI) and flow cytometry. The cells were incubated at -20°C for 24 hours in 75% ethanol, and then resuspended in 500 μL PBS, 2.5 μL RNaseA (10 mg/mL), and 5 μL PI (1 mg/mL) and allowed to incubate in the dark at 37°C for 20 minutes. The cells were then measured by a BD FACS Calibur flow cytometer (BD bioscience).

Cell sorting

After treatment with Olaparib or DMSO alone for 24 hours, 10^7 OVCAR8 cells were harvested, washed twice with PBS, and blocked with 3% BSA at 37 °C for 45 minutes. The cells were then stained with FITC-conjugated CD274 at 37 °C for 2 hours ($5 \mu\text{L}/2 \times 10^5$ cells in 100 μL 0.2% BSA). Then cells were washed with 1X PBS and immediately sorted using BD FACS Ariall (BD Biosciences, San Jose, CA, USA) flow cytometer. The positivity of CD274 antibody stain was determined by quadrant analysis as compared to the control (cells treated with DMSO alone were stained with the FITC-conjugated CD274 as the control).

Data mining

Using cBioportal (<http://cbioportal.org>) to analyze the data, an Ovarian Serous Cystadenocarcinoma (TCGA) research project based on 563 patients was analyzed as previously described (26). The correlation between *CD274* and *STAT3* target gene mRNA was analyzed using cBioportal as described (27).

Primary Human Ovarian Tissue Samples

In this study, 53 primary tumor samples were collected from patients diagnosed with ovarian cancer who underwent primary ovarian cancer surgery at Zhejiang University Hospital (Hangzhou, China). Only patients without preoperative radiotherapy or chemotherapy were enrolled in the study. All samples were obtained from tumor section without any adjacent normal tissue. Then formalin-fixed, paraffin embedded tissue cases were cut at 4 μ m thick sections and subjected to the following examinations. Tissue collection and analysis in this study were approved by the Ethics Committee of Women's Hospital of Zhejiang University, and written informed consent to perform the biological studies was obtained from all participants. All ovarian specimens were histologically verified by two pathologists independently.

Immunohistochemistry (IHC)

For histological analysis, human ovarian cancer tissues were paraffin-embedded. All slides were incubated with 3% hydrogen peroxide after deparaffinization and then were blocked by incubating in blocking buffer (5% goat serum in PBS) for 30 minutes. Slides were then probed with the anti-PARP1 diluted at 1:200 (Origene, #TA321380S), anti-PD-L1 diluted at 1:50 (Origene, #UM800121), anti-PAR, or anti-p-STAT3 followed by treatment with biotinylated secondary antibodies and horseradish peroxidase-conjugated avidin and were visualized with 3,3-diaminobenzidine following the manufacturer's protocol. All the reagents above were contained in anti-rabbit HRP-DAB Cell and Tissue Staining Kit (R&D Systems, #CTS005) and anti-mouse HRP-DAB Cell and Tissue

Staining Kit (R&D Systems, #CTS002). The digital images were quantified with the assistance of Image-Pro Plus 6.0 software (IPP, version 6.0, Media Cybernetics, CA, USA).

Statistical Analysis

All of the statistical data are presented as the mean \pm SD. Statistical significance of the differences was determined using Student's t-test. Significance was defined as $P < 0.05$. For immunohistochemistry analysis, the results were analyzed using Image-Pro Plus 6.0 software. For the evaluation of protein expression, the selected measurement parameter was integrated optical density (IOD). The optical density was calibrated systematically and the area of interest was extracted through the HSI mode, and the expression of each protein was calculated by IOD/tissue area, as described (28). Also, protein expression was evaluated by intensity scoring on scale of “–” to “+++” (–: no staining, +: weak staining, ++: moderate staining, +++: high staining) and proportion (0%, 1%-24%, 25-50%, >50%) (29). The P-value was calculated using the Pearson correlation test. The Student's t-test and Pearson correlations were analyzed by Prism 6 software (GraphPad Software Inc., La Jolla, CA, USA).

Results

PARP1 Suppresses the Transcription of PD-L1 in Cancer Cells

In addition to the biochemistry and molecular biology of PARP1 in DNA damage detection and repair, the mechanistic and functional understanding of the role of PARP1 in different biological processes has grown considerably (7). To investigate whether PARP1 is involved in cancer immune evasion, the ovarian cancer cell line OVCAR8 was transiently transfected with siRNA against PARP1, and we characterized a series of immunosuppressive factors, including genes encoding PD-L1, IL10, IL13, CXCL8, MIF, NOS2, COX2, B7H3, IDO, CD47, TIGIT, and CSF2 using qRT-PCR. PARP1 silencing led to an increase in PD-L1 mRNA (7.97-fold change, $P = 0.004$), as well as increases in expression of IL10 (2.47-fold change, $P = 0.18$), IL13 (2.25-fold change, $P = 0.26$), CXCL8

(1.88-fold change, $P=0.38$), MIF (2.04-fold change, $P=0.44$), COX2 (3.08-fold change, $P=0.25$), and TIGIT (1.36-fold change, $P=0.51$) (Fig. 1A and B). Among these affected genes, we were particularly interested in the alteration of PD-L1 gene expression, which may play a central role in the evasion of immune system of many cancer types (30).

To further confirm the involvement of PARP1 in PD-L1 regulation, we generated another siRNA PARP1-silenced ovarian cell line, SKOV3. PARP1-depleted SKOV3 cells also exhibited an enhanced transcription of PD-L1 mRNA (Fig. 1B). In parallel, the PD-L1 protein expression and cell surface PD-L1 expression were upregulated with PARP1 silencing (Fig. 1C and D). The impact of individual PARP1 siRNA on PD-L1 expression associated with the gene-silencing efficiency of the siRNA (Fig. 1B, C, and D), suggesting a PD-L1-associated defect. The increased PD-L1 expression in PARP1-depleted cells was also recapitulated in the breast cancer cell line MCF-7, the non-small cell lung carcinoma cell lines A549 and PC9, and the colon cancer cell lines Colo205 and SW620 (Supplementary Fig. S1). Taken together, these data suggest that PARP1 suppresses PD-L1 transcription in various cancer cells.

PARP1 Inhibits the Transcription of PD-L1 in a Catalytic-Dependent Manner

Considering that PARP1 controls the transcription of target genes, either with both catalytic-dependent and catalytic-independent mechanisms (31,32), PARP inhibitors that could efficiently suppress the catalytic activity of PARP1 were used to confirm whether PARP1-mediated PD-L1 expression was correlated to its catalytic activity. A significant elevation of PD-L1 mRNA expression was observed when OVCAR8 and SKOV3 cells were treated with 10 μ M olaparib for various times (Fig. 2A). To further test whether PARP inhibitors enhanced the transcription of PD-L1, we cloned the promoter region of PD-L1 downstream of a luciferase reporter gene (pGL4.14-PD-L1). The luciferase activity of the cells transfected with pGL4.14-PD-L1 was significantly increased when PARP1 was inhibited (Fig. 2B), and the protein expression of PD-L1 was upregulated by multiple PARP inhibitors in a dose-dependent manner (Supplementary Fig. S2A). To exclude the

impact of PARP1 on the degradation of PD-L1, cells were treated with olaparib, cycloheximide, or both for the indicated time. No significant difference in the kinetics of PD-L1 protein expression was observed between these two groups (Supplementary Fig. S2B). A similar upregulation of PD-L1 was observed with two additional PARP inhibitors, veliparib and A966492 (Fig. 2C and D). PARP inhibitors were unable to affect the fluorescence intensity of PD-L1 (Supplementary Fig. S2C and D). We also evaluated the expression of CD47, another cell surface immunosuppressive factor, which was not altered at the mRNA level upon PARP1 silencing (Fig. 1A), and the cell surface expression of CD47 was not significantly affected by the PARP inhibitor olaparib (Supplementary Fig. S2E). Neither cell viability nor apoptosis was affected by PARP inhibitors at indicated concentrations (Supplementary Fig. S3). The reconstitution of siRNA-resistant, wild-type PARP1 attenuated the expression of PD-L1 in siPARP1 (PARP1-silenced) cells to a level similar seen in scramble cells (Fig. 2E), whereas the reconstitution of the mutant PARP1 failed to attenuate PD-L1 expression. These data suggest that the inhibition of PD-L1 transcription by PARP1 depends on its catalytic activity.

STAT3 Is Required for PARP1-Mediated PD-L1 Expression

We next asked how PARP1 regulated PD-L1 transcription. Studies indicate that the PARylation of transcriptional factors by PARP1 can alter or modulate their activities, playing a critical role in gene regulation (33). We hypothesized that this function might also apply to PARP1-modulated PD-L1 transcription. Thus, we silenced the transcription factors STAT1, STAT3, and MYC (34-36), which have been reported to regulate PD-L1 transcription by directly binding to its promoter region. We found that PD-L1 expression induced by PARP1 inhibition was not affected by STAT1 and MYC deficiency but was abolished with the silencing of STAT3 (Fig. 3A). In parallel, PARP1 inhibition promoted PD-L1 transcription, which was attenuated by STAT3 silencing (Fig. 3B). Similar results were obtained with the OVCAR8 and MCF-7 cells (Supplementary Fig. S4A and B).

These data suggest a major contribution of STAT3 to PARP1-mediated PD-L1 transcription.

To further confirm the involvement of STAT3 in PARP1-mediated PD-L1 transcription, SKOV3 cells were transfected with pGL4.14-PD-L1, Flag-PARP1, and HA-STAT3, as indicated for 36 hours. The PD-L1 luciferase activity was upregulated more than 5-fold compared with the vector when transfected with HA-STAT3, whereas it was significantly downregulated when co-transfected with Flag-PARP1 (Fig. 3C). We also performed a ChIP assay using a PCR primer set capable of amplifying the promoter region of PD-L1 containing the STAT3 binding sites. The direct binding of STAT3 to the PD-L1 promoter was observed in SKOV3 cells, and this binding was significantly enhanced by PARP1 inhibition (Fig. 3D). We analyzed an ovarian serous cystadenocarcinoma dataset containing 563 samples from TCGA, based on the large-scale cancer genomics datasets provided by cBioPortal. The mRNA expression of MCL1, CCL5, IFN γ , IL4R, and IL2RA, five well-known STAT3 target genes, was correlated with mRNA expression of CD274 (Supplementary Fig. S4C), further suggesting that the expression of PD-L1 is positively associated with STAT3 activity. These data collectively revealed that PARP1 regulates PD-L1 expression through STAT3.

STAT3 Is PARylated by PARP1

We then asked whether PARP1 directly poly(ADP-ribose)ylated STAT3 to inhibit its transcriptional activity. To test this hypothesis, we first determined if PARP1 could form complexes with STAT3 in cancer cells. Pull-down assays validated the direct endogenous interaction of PARP1 with endogenous STAT3 (Fig. 4A). This interaction was further confirmed with the ectopic expression of PARP1 or STAT3 (Fig. 4B). PARP1 inhibition also disrupted the interaction between PARP1 and STAT3 (Fig. 4B). Because endogenous PARylation was scarcely detected, we used an ectopic expression system to study the ADP-ribosylation of STAT3. Auto-modification of PARP1 is a well-documented phenomenon (37). To distinguish whether the PAR signal was coming from STAT3 and

not from auto-modified PARP1, we extracted proteins using a 4% SDS lysis buffer to abolish the interaction between PARP1 and STAT3 but not the covalent PARylation of STAT3 (38). As expected, PAR was pulled down with STAT3 protein, and PARylation of STAT3 was observed, as the molecular weight smear signals began with 92 KD, indicating that PAR signal came directly from STAT3 (Fig. 4C). The PARylation of STAT3 was also observed in STAT3-containing immunoprecipitates from HEK 293T cells ectopically expressing HA-STAT3 and Flag-PARP1 (Fig. 4D), which was abolished by PARP1 inhibition. Taken together, these results demonstrated that STAT3 is PARylated by PARP1.

PARP1 Inhibits the Transcription of PD-L1 by PARylating STAT3

It remains to be determined if the role of PARP1-mediated PD-L1 transcription is due to the PARylation of STAT3. Previous studies have identified that the glutamate (E988) and histidine (H862) are the residues responsible for the polymerase activity of PARP1 (39). We generated point mutations in the PARP1 gene at positions histidine (H862) and glutamate (E988) respectively. Compared to the group transfected with wild-type PARP1, the PARylation of STAT3 was not observed when the cells were transfected with the H862 or E988 mutants (Fig. 5A). We then analyzed the effect of mutated PARP1 on the transcription of PD-L1. Mutated PARP1 could not suppress STAT3-mediated PD-L1 promoter activity due to loss of its polymerase activity (Fig. 5B), and in both the SKOV3 and OVCAR8 cell lines, PARP1 inactivation did not downregulate PD-L1 protein expression (Fig. 5C and D). These data indicated that PARP1 inhibits PD-L1 transcription through the PARylation of STAT3.

The Crosstalk Between PARylation and Phosphorylation

Tyrosine phosphorylation is an important post-translational modification of STAT3, which functions as a switching signal to activate STAT3. The tyrosine phosphorylation of STAT3 is required for its dimerization, nuclear translocation, and DNA binding (40). Thus, we next assessed whether PARP1 affected the tyrosine phosphorylation of STAT3. The silencing

or pharmacological inhibition of PARP1 enhanced the phosphorylation of STAT3 in SKOV3 and OVCAR8 cell lines (Fig. 6A and B). In parallel, a significant increase in the nucleus localization of STAT3 was observed, further suggesting the activation of STAT3 (Fig. 6C), and the constitution of wild-type PARP1 significantly attenuated the phosphorylation of STAT3 caused by PARP1 silencing (Fig. 6D). Using two-color flow cytometry, we found that PARP1 silenced cells exhibited a significant increase in the proportion cells positive for both phosphorylated (p) STAT3 and PD-L1 (13.34% and 15.74% of the total cell count) compared to control groups (3.10% and 2.62%) after 24 hours (Supplementary Fig. S5A and B). The increased STAT3 phosphorylation of PARP1-deficient cells was also recapitulated in the breast cancer cell line MCF-7, the non-small cell lung carcinoma cell lines A549 and PC9, and the colon cancer cell lines Colo205 and SW620 (Supplementary Fig. S6). Shiping Jiao et al. also report that a PARP inhibitor upregulated the expression of PD-L1 in breast cancer (41), and they attribute the induction of PD-L1 to GSK3 β inactivation, an off-target activity of PARP inhibitors. To determine whether this mechanism is also involved, we evaluated GSK3 β activity in our system. Our data showed that the PARP inhibitor does not affect the phosphorylation of GSK3 β in ovarian cancer (Supplementary Fig. S6E). These data suggest that PARP1 acts as a suppressor of STAT3 phosphorylation in various cancer cells.

STATs are phosphorylated by JAK2, and they then dimerize and translocate to the nucleus, where they activate gene transcription. Our data showed that JAK2 phosphorylation was not affected by PARP1 silencing (Fig. 6E). Thus, we inferred that PARP1-mediated PARylation might affect the de-phosphorylation process of STAT3. Cells were first transfected with Flag-PARP1 for 24 hours, and then 500 μ M vanadate, a general inhibitor for tyrosine phosphatases, was added for 25 minutes. Overexpression of PARP1 could not reduce the phosphorylation of STAT3 in the presence of vanadate (Fig. 6F). These results indicated that PARylation increases de-phosphorylation of STAT3.

We then generated STAT3 with a Y705F mutation (mutation of tyrosine 705 into phenylalanine, leading to activation deficiency) and a constitutively active STAT3

(STAT3C). This mutant has STAT3 constitutively active as a result of substituting the cysteine residues (C661A and C663N), allowing STAT3 dimerization and activation. The PARylation signal could not be detected when transfected with STAT3Y705F. However, a PARylation signal was detected in STAT3C cells. The smear signal of STAT3 was consistent with its phosphorylation (Fig. 6G). Alternatively, we employed another assay, in which the cells were transfected with Flag-PARP1 and HA-STAT3 followed by treatment with 5 μ M AZD1480 (JAK2 inhibitor) for 12 hours. The phosphorylation of STAT3 was efficiently inhibited by AZD1480, while the PARylation of STAT3 was significantly reduced (Fig. 6H). Taken together, these results indicated that PARP1 was prone to bind the active form of STAT3.

Correlation Between the Expression of PARP1 and PD-L1, p-STAT3, and PAR

To further validate our findings in human cancer patient samples, we analyzed the correlation between the expression of PARP1 and PD-L1 in human ovarian cancer specimens using immunohistochemistry (IHC). High PARP1 protein was detected in 24 (58.5%) of the 41 specimens, of which, 23 (56.1%) cases showed low PD-L1 expression (Fig. 7A). The Pearson chi-square test further showed an inverse correlation between PARP1 and PD-L1 expression in human cancer patient specimens ($P=0.0002$, $r=-0.54783$). These results suggest a connection between high PARP1 expression and low PD-L1 expression in primary ovarian cancer tissues.

To explore the correlation between PARylation and STAT3, cell sorting was used to separate low and high PD-L1 expression cells after PARP1 inhibitor administration. High PD-L1 expression associated with higher p-STAT3 (Supplementary Fig. S7A and B). After culturing for another 72 hours (to return to baseline), a stronger smear band was observed in high PD-L1-expressing cells (Supplementary Fig. S7C), suggesting that the response by cells to PARP1 inhibition might due to their high basal PARP1 catalytic activity. IHC of ovarian cancer patient tissues ($n=53$) was used to define PAR and p-STAT3 levels and found PAR and p-STAT3 both were found in the nucleus. (Fig. 7B). An inverse correlation

was found between PARylation and p-STAT3 expression ($P < 0.0001$, $r = -0.8953$). Our results suggest that PARP1-mediated PARylation might affect PD-L1 by suppressing STAT3 activity.

Discussion

In the current study, we determined that STAT3, a key oncogenic transcriptional factor, could be poly(ADP-ribosyl)ated by PARP1. We discovered a crosstalk between PARylation and phosphorylation. Currently, very few examples of definitive biological roles for the PARylation of proteins exist in the literature. Our results provide a clear example of how the ADP-ribosylation of a key transcription factor can affect the molecular and biochemical function of a protein, as well as the biological outcomes that it controls. More broadly, our results connected PARP1-dependent PARylation to the regulation of cancer immune suppression.

Increasing evidence exists showing that the expression of PD-L1 is mediated by the oncogenic activation of signaling pathways and is also regulated by factors in the tumor microenvironment (12,42,43). Signaling pathways drive PD-L1 expression primarily by transcriptional upregulation. Among the transcriptional factors involved, STAT3 has been identified as a critical regulator of PD-L1 expression in various cell systems. PD-L1 is transcriptionally regulated by STAT3 and MYC in ALK-negative anaplastic large cell lymphoma (21). The AKT-STAT3 pathway regulates the expression of PD-L1 on non-small lung cancers with aberrant EGFR activity (44), and STAT3 regulates PD-L1 expression in chemotherapy-resistant lung squamous cell carcinoma (45). In nasopharyngeal carcinoma, latent membrane protein-1 enhances PD-L1 expression with a concomitant increase in phosphorylated STAT3 (46). Here, we reported that PARP1 suppressed PD-L1 expression through the PARylation of STAT3, which could be found in various cancer cells. This finding differs from previous studies and provides a negative regulation pattern of PD-L1 in cancers. In this regard, the regulation of PARP1 activity would be important for the expression of PD-L1. Although DNA strand breaks are potent

stimuli of PARP1 enzymatic activity, the context-dependent mechanism regulating PARP1 activation and signaling is poorly understood. Studies suggest that, despite similar expression, PARP1 is differentially activated in cell lines under genotoxic conditions, which generates signaling outputs with substantial heterogeneity (47). This could indicate that the upregulation of PD-L1 differs in various cancer cells. Taken together, our findings suggest that PARP1 potentially safeguards PD-L1 by suppressing STAT3 activity and that the loss of PARP1 suppression might be another mechanism for elevated PD-L1 expression in cancer cells.

STAT3 is constitutively activated by the phosphorylation of tyrosine 705 and serine 727 in a variety of cancers because of the expression of oncoproteins and tumor-produced factors. Phosphorylated STAT3 monomers form homo- or heterodimers and translocate to the nucleus where they bind to specific sequences in the promoters of target genes to regulate gene transcription (48). The activity of STAT3 could also be negatively regulated by tyrosine phosphatases, which inhibit STAT3 phosphorylation (49). In this study, we observed that silencing or inhibition of PARP1 enhanced the phosphorylation of STAT3, which was reversed by reconstitution of wild-type PARP1. Phosphorylated JAK2 was not affected by PARP1 silencing or inhibition, but treating with vanadate, a general inhibitor for tyrosine phosphatases, blocked the effects of PARP1 on de-phosphorylation of STAT3. Based on this, we concluded that PARP1-mediated PARylation might affect the de-phosphorylation process of STAT3. However, how ADP-ribosylation affects the behavior of tyrosine phosphatases needs further investigation. Here, we showed that PARylation is another post-translational modification of STAT3 that reduces the activity of STAT3. Whether this is an important negative regulation mechanism for STAT3 is worth further study.

Among the post-translational modifications, only the crosstalk between ADP-ribosylation and ubiquitylation has been reported (50). An example of this is PAR-dependent ubiquitylation, a process in which the PARylation of a protein serves as a signal for its subsequent ubiquitylation, which may then lead to the ubiquitin-dependent degradation of

the protein by the proteasome (51). PAR-dependent ubiquitylation is likely to be a general mechanism controlling the stability and degradation of many PARP substrate proteins. Our findings reveal a crosstalk between PARylation and phosphorylation. It will be of interest to determine whether this is also a general mechanism regulating the activity of PARP substrate proteins.

Over the decades, PARP1 has been studied as the key DNA damage repair enzyme and has now become an attractive target for cancer therapy (37). A large number of PARP inhibitors are in clinical studies, and several of them have been approved for the clinical therapy of ovarian cancer. However, our study suggests that the application of PARP inhibitors in various cancers promotes the transcription of PD-L1. Whether this effect will lead to cancer evasion during treatment with PARP inhibitors should be evaluated. Our data also showed that silencing of PARP1 enhanced the transcription of PD-L1 in two breast cancer cell lines. It should be noted that in Shiping Jiao's study, they showed an inverse correlation between the PARylation and PD-L1 expression in clinical breast cancer samples, which partially supports our findings concerning the regulation of PD-L1 by PARP-mediated ADP-ribosylation.

Taken together, our study revealed that PARP1 attenuates the transcription of PD-L1 through the PARylation of STAT3 and subsequently de-phosphorylation of STAT3 (Fig. 7C). Our study not only provided insights into the biological function of PARP1, thereby uncovering a new regulatory mechanism of PD-L1, but also provided new ideas and strategies to improve the clinical therapies used for ovarian cancer.

Acknowledgements

This work was supported by National Natural Science Foundation of China (for Distinguished Young Scholar, No. 81625024 to Yang B.); National Natural Science Foundation of China (No. 81773754 and No. 81573428 to Ding L.).

References

1. Gibson BA, Kraus WL. New insights into the molecular and cellular functions of poly(ADP-ribose) and PARPs. *Nat Rev Mol Cell Biol* **2012**;13(7):411-24 doi 10.1038/nrm3376.
2. Gupte R, Liu Z, Kraus WL. PARPs and ADP-ribosylation: recent advances linking molecular functions to biological outcomes. *Genes Dev* **2017**;31(2):101-26 doi 10.1101/gad.291518.116.
3. Gibson BA, Zhang Y, Jiang H, Hussey KM, Shrimp JH, Lin H, *et al.* Chemical genetic discovery of PARP targets reveals a role for PARP-1 in transcription elongation. *Science* **2016**;353(6294):45-50 doi 10.1126/science.aaf7865.
4. Lonn P, van der Heide LP, Dahl M, Hellman U, Heldin CH, Moustakas A. PARP-1 attenuates Smad-mediated transcription. *Mol Cell* **2010**;40(4):521-32 doi 10.1016/j.molcel.2010.10.029.
5. Luo X, Nie J, Wang S, Chen Z, Chen W, Li D, *et al.* Poly(ADP-ribosylation) of FOXP3 Protein Mediated by PARP-1 Protein Regulates the Function of Regulatory T Cells. *J Biol Chem* **2015**;290(48):28675-82 doi 10.1074/jbc.M115.661611.
6. Luo X, Ryu KW, Kim DS, Nandu T, Medina CJ, Gupte R, *et al.* PARP-1 Controls the Adipogenic Transcriptional Program by PARylating C/EBPbeta and Modulating Its Transcriptional Activity. *Mol Cell* **2017**;65(2):260-71 doi 10.1016/j.molcel.2016.11.015.
7. Bock FJ, Chang P. New directions in poly(ADP-ribose) polymerase biology. *FEBS J* **2016**;283(22):4017-31 doi 10.1111/febs.13737.
8. Dong H, Strome SE, Salomao DR, Tamura H, Hirano F, Flies DB, *et al.* Tumor-associated B7-H1 promotes T-cell apoptosis: a potential mechanism of immune evasion. *Nat Med* **2002**;8(8):793-800 doi 10.1038/nm730.
9. Freeman GJ, Long AJ, Iwai Y, Bourque K, Chernova T, Nishimura H, *et al.* Engagement of the PD-1 immunoinhibitory receptor by a novel B7 family member leads to negative regulation of lymphocyte activation. *J Exp Med* **2000**;192(7):1027-34.
10. Clark CA, Gupta HB, Sareddy G, Pandeswara S, Lao S, Yuan B, *et al.* Tumor-Intrinsic PD-L1 Signals Regulate Cell Growth, Pathogenesis, and Autophagy in Ovarian Cancer and Melanoma. *Cancer Res* **2016**;76(23):6964-74 doi 10.1158/0008-5472.CAN-16-0258.
11. Bertucci F, Goncalves A. Immunotherapy in Breast Cancer: the Emerging Role of PD-1 and PD-L1. *Curr Oncol Rep* **2017**;19(10):64 doi 10.1007/s11912-017-0627-0.
12. Wang J, Jia Y, Zhao S, Zhang X, Wang X, Han X, *et al.* BIN1 reverses PD-L1-mediated immune escape by inactivating the c-MYC and EGFR/MAPK signaling pathways in non-small cell lung cancer. *Oncogene* **2017** doi 10.1038/onc.2017.217.

13. Masugi Y, Nishihara R, Yang J, Mima K, da Silva A, Shi Y, *et al.* Tumour CD274 (PD-L1) expression and T cells in colorectal cancer. *Gut* **2017**;66(8):1463-73 doi 10.1136/gutjnl-2016-311421.
14. Pardoll DM. The blockade of immune checkpoints in cancer immunotherapy. *Nat Rev Cancer* **2012**;12(4):252-64 doi 10.1038/nrc3239.
15. Zou W, Wolchok JD, Chen L. PD-L1 (B7-H1) and PD-1 pathway blockade for cancer therapy: Mechanisms, response biomarkers, and combinations. *Sci Transl Med* **2016**;8(328):328rv4 doi 10.1126/scitranslmed.aad7118.
16. Brahmer JR, Tykodi SS, Chow LQ, Hwu WJ, Topalian SL, Hwu P, *et al.* Safety and activity of anti-PD-L1 antibody in patients with advanced cancer. *N Engl J Med* **2012**;366(26):2455-65 doi 10.1056/NEJMoa1200694.
17. Topalian SL, Hodi FS, Brahmer JR, Gettinger SN, Smith DC, McDermott DF, *et al.* Safety, activity, and immune correlates of anti-PD-1 antibody in cancer. *N Engl J Med* **2012**;366(26):2443-54 doi 10.1056/NEJMoa1200690.
18. Chen J, Jiang CC, Jin L, Zhang XD. Regulation of PD-L1: a novel role of pro-survival signalling in cancer. *Ann Oncol* **2016**;27(3):409-16 doi 10.1093/annonc/mdv615.
19. Noman MZ, Desantis G, Janji B, Hasmim M, Karray S, Dessen P, *et al.* PD-L1 is a novel direct target of HIF-1alpha, and its blockade under hypoxia enhanced MDSC-mediated T cell activation. *J Exp Med* **2014**;211(5):781-90 doi 10.1084/jem.20131916.
20. Marzec M, Zhang Q, Goradia A, Raghunath PN, Liu X, Paessler M, *et al.* Oncogenic kinase NPM/ALK induces through STAT3 expression of immunosuppressive protein CD274 (PD-L1, B7-H1). *Proc Natl Acad Sci U S A* **2008**;105(52):20852-7 doi 10.1073/pnas.0810958105.
21. Atsaves V, Tsesmetzis N, Chioureas D, Kis L, Leventaki V, Drakos E, *et al.* PD-L1 is commonly expressed and transcriptionally regulated by STAT3 and MYC in ALK-negative anaplastic large-cell lymphoma. *Leukemia* **2017**;31(7):1633-7 doi 10.1038/leu.2017.103.
22. Fang W, Zhang J, Hong S, Zhan J, Chen N, Qin T, *et al.* EBV-driven LMP1 and IFN-gamma up-regulate PD-L1 in nasopharyngeal carcinoma: Implications for oncotargeted therapy. *Oncotarget* **2014**;5(23):12189-202 doi 10.18632/oncotarget.2608.
23. Casey SC, Tong L, Li Y, Do R, Walz S, Fitzgerald KN, *et al.* MYC regulates the antitumor immune response through CD47 and PD-L1. *Science* **2016**;352(6282):227-31 doi 10.1126/science.aac9935.
24. Liu Y, Deisseroth A. Oncolytic adenoviral vector carrying the cytosine deaminase gene for melanoma gene therapy. *Cancer Gene Ther* **2006**;13(9):845-55 doi 10.1038/sj.cgt.7700962.
25. Ding L, Liang G, Yao Z, Zhang J, Liu R, Chen H, *et al.* Metformin prevents cancer metastasis by inhibiting M2-like polarization of tumor associated macrophages. *Oncotarget* **2015**;6(34):36441-55 doi

- 10.18632/oncotarget.5541.
26. Bell D, Berchuck A, Birrer M, Chien J, Cramer DW, Dao F, *et al.* Integrated genomic analyses of ovarian carcinoma. *Nature* **2011**;474(7353):609-15 doi 10.1038/nature10166.
27. Gao JJ, Aksoy BA, Dogrusoz U, Dresdner G, Gross B, Sumer SO, *et al.* Integrative Analysis of Complex Cancer Genomics and Clinical Profiles Using the cBioPortal. *Science Signaling* **2013**;6(269) doi ARTN p11
DOI 10.1126/scisignal.2004088.
28. Zhong CJ, Duan LP, Wang K, Xu ZJ, Ge Y, Yang CQ, *et al.* Esophageal intraluminal baseline impedance is associated with severity of acid reflux and epithelial structural abnormalities in patients with gastroesophageal reflux disease. *Journal of Gastroenterology* **2013**;48(5):601-10 doi 10.1007/s00535-012-0689-6.
29. Al-Batran SE, Rafiyan MR, Atmaca A, Neumann A, Karbach J, Bender A, *et al.* Intratumoral T-cell infiltrates and MHC class I expression in patients with stage IV melanoma. *Cancer Research* **2005**;65(9):3937-41 doi Doi 10.1158/0008-5472.Can-04-4621.
30. Dong H, Chen L. B7-H1 pathway and its role in the evasion of tumor immunity. *J Mol Med (Berl)* **2003**;81(5):281-7 doi 10.1007/s00109-003-0430-2.
31. Kraus WL, Hottiger MO. PARP-1 and gene regulation: progress and puzzles. *Mol Aspects Med* **2013**;34(6):1109-23 doi 10.1016/j.mam.2013.01.005.
32. Krishnakumar R, Kraus WL. The PARP side of the nucleus: molecular actions, physiological outcomes, and clinical targets. *Mol Cell* **2010**;39(1):8-24 doi 10.1016/j.molcel.2010.06.017.
33. Gibson BA, Kraus WL. New insights into the molecular and cellular functions of poly(ADP-ribose) and PARPs. *Nature Reviews Molecular Cell Biology* **2012**;13(7):411-24 doi 10.1038/nrm3376.
34. MYC Promotes Tumorigenesis via Activation of CD47 and PD-L1. *Cancer Discov* **2016**;6(5):472 doi 10.1158/2159-8290.CD-RW2016-051.
35. Koh J, Jang JY, Keam B, Kim S, Kim MY, Go H, *et al.* EML4-ALK enhances programmed cell death-ligand 1 expression in pulmonary adenocarcinoma via hypoxia-inducible factor (HIF)-1 alpha and STAT3. *Oncoimmunology* **2016**;5(3) doi ARTN e1108514
10.1080/2162402X.2015.1108514.
36. Hirahara K, Ghoreschi K, Yang XP, Takahashi H, Laurence A, Vahedi G, *et al.* Interleukin-27 Priming of T Cells Controls IL-17 Production In trans via Induction of the Ligand PD-L1. *Immunity* **2012**;36(6):1017-30 doi 10.1016/j.immuni.2012.03.024.
37. Rouleau M, Patel A, Hendzel MJ, Kaufmann SH, Poirier GG. PARP inhibition: PARP1 and beyond. *Nature Reviews Cancer* **2010**;10(4):293-301 doi 10.1038/nrc2812.

38. Xiao Y, Pollack D, Nieves E, Winchell A, Callaway M, Vigodner M. Can your protein be sumoylated? A quick summary and important tips to study SUMO-modified proteins. *Anal Biochem* **2015**;477:95-7 doi 10.1016/j.ab.2014.11.006.
39. Barkauskaite E, Jankevicius G, Ahel I. Structures and Mechanisms of Enzymes Employed in the Synthesis and Degradation of PARP-Dependent Protein ADP-Ribosylation. *Molecular Cell* **2015**;58(6):935-46 doi 10.1016/j.molcel.2015.05.007.
40. Shuai K, Liu B. Regulation of JAK-STAT signalling in the immune system. *Nat Rev Immunol* **2003**;3(11):900-11 doi 10.1038/nri1226.
41. Jiao S, Xia W, Yamaguchi H, Wei Y, Chen MK, Hsu JM, *et al.* PARP Inhibitor Upregulates PD-L1 Expression and Enhances Cancer-Associated Immunosuppression. *Clin Cancer Res* **2017**;23(14):3711-20 doi 10.1158/1078-0432.CCR-16-3215.
42. Sumimoto H, Imabayashi F, Iwata T, Kawakami Y. The BRAF-MAPK signaling pathway is essential for cancer-immune evasion in human melanoma cells. *J Exp Med* **2006**;203(7):1651-6 doi 10.1084/jem.20051848.
43. Jiang X, Zhou J, Giobbie-Hurder A, Wargo J, Hodi FS. The activation of MAPK in melanoma cells resistant to BRAF inhibition promotes PD-L1 expression that is reversible by MEK and PI3K inhibition. *Clin Cancer Res* **2013**;19(3):598-609 doi 10.1158/1078-0432.CCR-12-2731.
44. Abdelhamed S, Ogura K, Yokoyama S, Saiki I, Hayakawa Y. AKT-STAT3 Pathway as a Downstream Target of EGFR Signaling to Regulate PD-L1 Expression on NSCLC cells. *J Cancer* **2016**;7(12):1579-86 doi 10.7150/jca.14713.
45. Fujita Y, Yagishita S, Hagiwara K, Yoshioka Y, Kosaka N, Takeshita F, *et al.* The clinical relevance of the miR-197/CKS1B/STAT3-mediated PD-L1 network in chemoresistant non-small-cell lung cancer. *Mol Ther* **2015**;23(4):717-27 doi 10.1038/mt.2015.10.
46. Carbotti G, Barisione G, Airoidi I, Mezzanzanica D, Bagnoli M, Ferrero S, *et al.* IL-27 induces the expression of IDO and PD-L1 in human cancer cells. *Oncotarget* **2015**;6(41):43267-80 doi 10.18632/oncotarget.6530.
47. Zhen Y, Zhang Y, Yu Y. A Cell-Line-Specific Atlas of PARP-Mediated Protein Asp/Glu-ADP-Ribosylation in Breast Cancer. *Cell Rep* **2017**;21(8):2326-37 doi 10.1016/j.celrep.2017.10.106.
48. Heinrich PC, Behrmann I, Haan S, Hermanns HM, Muller-Newen G, Schaper F. Principles of interleukin (IL)-6-type cytokine signalling and its regulation. *Biochem J* **2003**;374(Pt 1):1-20 doi 10.1042/BJ20030407.
49. Bard-Chapeau EA, Li SW, Ding J, Zhang SS, Zhu HH, Princen F, *et al.* Ptpn11/Shp2 Acts as a Tumor Suppressor in Hepatocellular Carcinogenesis. *Cancer Cell* **2011**;19(5):629-39 doi 10.1016/j.ccr.2011.03.023.
50. Wang Z, Michaud GA, Cheng Z, Zhang Y, Hinds TR, Fan E, *et al.* Recognition of the iso-ADP-ribose moiety in poly(ADP-ribose) by WWE domains suggests a

general mechanism for poly(ADP-ribosyl)ation-dependent ubiquitination. *Genes Dev* **2012**;26(3):235-40 doi 10.1101/gad.182618.111.

51. Kashima L, Idogawa M, Mita H, Shitashige M, Yamada T, Ogi K, *et al.* CHFR protein regulates mitotic checkpoint by targeting PARP-1 protein for ubiquitination and degradation. *J Biol Chem* **2012**;287(16):12975-84 doi 10.1074/jbc.M111.321828.

Figure Legends

Figure 1. PARP1 suppresses the transcription of PD-L1 in cancer cells. **A**, Heat map showing the mRNA fold change when PARP1 was silenced. The transcription of immunosuppressive factors was analyzed by qRT-PCR in the human ovarian cancer cell line OVCAR8 when PARP1 was downregulated by siRNA (siPARP1). **B**, The PD-L1 mRNA expression was measured in OVCAR8 and SKOV3 cells transfected with siRNA-negative control (NC) and siPARP1. **C**, PD-L1 protein expression with PARP1 silenced. The PD-L1 protein expression was determined by Western blot in OVCAR8 and SKOV3 cells when treated with PARP1 siRNA-negative control (NC) and siPARP1. **D**, Cell surface PD-L1 expression with PARP1 silenced in both OVCAR8 and SKOV3 cell lines. Cell surface PD-L1 was measured by flow cytometry in OVCAR8 and SKOV3 cells when the cells were treated with siRNA-negative control (NC) and siPARP1. Cells were assessed for PD-L1 or mouse IgG control antibody (IgG). The data are presented as the mean \pm SD of triplicate experiments. Statistical significance was determined by Student's t-test. *** P <0.001; ** P <0.01; * P <0.05.

Figure 2. PARP1 inhibits the transcription of PD-L1 in a catalytic-dependent manner. **A**, 3×10^5 OVCAR8 and SKOV3 cells were treated with olaparib (10 μ M) for 0, 4, 8, 12, and 24 hours, and the level of PD-L1 mRNA was measured by qRT-PCR. **B**, Cells transfected with a PD-L1 promoter report gene were treated with olaparib (10 μ M) for 24 hours, and their luciferase activity was detected using the Dual-Luciferase Reporter Assay System. **C**, 3×10^5 OVCAR8 and SKOV3 cells were treated with the indicated PARP inhibitors or with DMSO alone, and PD-L1 mRNA was quantified by qRT-PCR. **D**, Cell

surface PD-L1 was measured by flow cytometry after the 3×10^5 OVCAR8 and SKOV3 cells were treated with the indicated PARP inhibitors. Cell lines were assessed for CD274 or mouse IgG control antibody (IgG). **E**, The reconstitution of PARP1 in PARP1-silenced OVCAR8 cells. The cells were transfected with PARP1 siRNA or siRNA-negative control (NC), followed by the ectopic expression of siRNA-resistant wild-type PARP1 or mutant PARP1 (H862 or E988), as indicated, for 24 hours. Cell surface PD-L1 was measured by flow cytometry. The data are presented as the mean \pm SD of triplicate determinations. Statistical significance was determined by Student's t-test. *** $P < 0.001$; ** $P < 0.01$; * $P < 0.05$; n.s: not significant.

Figure 3. STAT3 is required for PARP1-mediated PD-L1 expression. **A**, PARP1 inhibition-induced PD-L1 expression after STAT1, MYC, and STAT3 silencing. PD-L1 protein expression in SKOV3 cells was analyzed after treatment with olaparib (10 μ M) alone or in the presence of STAT1, MYC, or STAT3 siRNA or siRNA-negative control (NC). SKOV3 were assessed for CD274 or mouse IgG control antibody (IgG) via flow cytometry. **B**, The PD-L1 mRNA measured via qRT-PCR when 3×10^5 SKOV3 cells were treated with olaparib (10 μ M) alone or in the absence of STAT3. **C**, The SKOV3 cells were transfected the PD-L1 promoter reporter gene, which was followed by the introduction of Flag-PARP1, HA-STAT3, or both for 36 hours. PD-L1 luciferase activity was determined. **D**, Binding of STAT3 to the PD-L1 promoter after PARP1 inhibition. 4×10^6 SKOV3 cells were treated with olaparib (10 μ M) for 24 hours. Cell lysates were then analyzed using a ChIP assay with an STAT3 rabbit polyclonal antibody and primer pairs specific for the *CD274* gene promoter. Non-immunoprecipitated lysates (input) and immunoprecipitates obtained with the anti-rabbit IgG served as positive and negative controls, respectively. Control (Con): cells treated with DMSO alone. The data are presented as the mean \pm SD of triplicate determinations. Statistical significance was determined by Student's t-test. *** $P < 0.001$; ** $P < 0.01$; ## $P < 0.01$.

Figure 4. STAT3 is poly(ADP-ribosyl)ated by PARP1. **A**, The interaction between endogenous STAT3 and PARP1. The HEK 293T cells lysates were immunoprecipitated with anti-PARP1, which was followed by immunoblotting with the STAT3 antibody. **B**, The reciprocal immunoprecipitation of PARP1 and STAT3. HEK 293T cells were transfected with Flag-PARP1 or HA-STAT3. The cell lysates were immunoprecipitated with the anti-Flag or anti-HA, which was followed by immunoblotting with different antibodies as indicated. **C**, HEK 293T cells were transfected with empty vector, Flag-PARP1, HA-STAT3, or both. The cell lysates were immunoprecipitated with the anti-PAR and detected by the anti-HA. **D**, HEK293T cells were co-transfected with plasmids, as indicated, and were treated with olaparib for 36 hours. The cell lysates were immunoprecipitated with the anti-HA, and the poly(ADP-ribosyl)ated STAT3 proteins were detected using an anti-PAR.

Figure 5. PARP1 Inhibits the transcription of PD-L1 by poly(ADP-ribosyl)ating STAT3. **A**, HEK 293T cells were transfected with HA-STAT3, together with wild-type Flag-PARP1 or the catalytic mutant Flag-PARP1 (H862 or E988). After 36 hours, the cells were subjected to immunoprecipitation with anti-HA, followed by Western blot to detect poly(ADP-ribosyl)ated STAT3. **B**, SKOV3 cells were transfected with the PD-L1 promoter report gene, together with wild Flag-PARP1, mutant Flag-PARP1 (H862 or E988), and HA-STAT3 as indicated. The luciferase activity was measured 36 hours after transfection. **C-D**, PD-L1 protein in OVCAR8 and SKOV3 cells was determined by flow cytometry after transfection with wild Flag-PARP1, mutant Flag-PARP1 (H862 or E988), and HA-STAT3 as indicated. Statistical significance was determined by Student's t-test. The data are presented as the mean \pm SD of triplicate determinations. *** P <0.001; ** P <0.01; n.s: not significant.

Figure 6. The crosstalk between PARylation and phosphorylation. **A**, 3×10^5 SKOV3 and OVCAR8 cells were treated with PARP1 siRNA (siPARP1) for 24 hours, and the

phosphorylation of STAT3 was analyzed by Western blot. **B**, OVCAR8 cells were treated with various PARP inhibitors for 24 hours, and the phosphorylation of STAT3 was analyzed by Western blot. **C**, The analysis of STAT3 distribution by confocal microscopy. SKOV3 cells were stained with anti-STAT3 and DAPI. Scale bar: 25 μ m. **D**, PARP1 siRNA-treated OVCAR8 cells were transfected with siRNA-resistant wild Flag-PARP1 or mutant Flag-PARP1 (H862 or E988), and the phosphorylation of STAT3 was assessed by Western blot. **E**, SKOV3 and OVCAR8 cells were treated with siPARP1 for 24 hours, and the phosphorylation of JAK2 was analyzed by Western blot. **F**, OVCAR8 cells were first transfected with Flag-PARP1 for 24 hours, and then 500 μ M vanadate was added for 25 minutes, and the phosphorylation of STAT3 was analyzed by Western blot, GA: GAPDH. **G**, HEK 293T cells were transfected with Flag-PARP1, together with HA-STAT3, a constitutively active STAT3 (HA-STAT3C), or the activation mutant HA-STAT3Y705F. The cells were subjected to immunoprecipitation with anti-HA, followed by Western blot to detect poly(ADP-ribosyl)ated STAT3. IB: immunoblotting. **H**, HEK 293T cells were transfected with Flag-PARP1 and HA-STAT3 followed by treatment with 5 μ M AZD1480 (JAK2 inhibitor) for 12 hours. Western blot was used to detect poly(ADP-ribosyl)ated STAT3. NC: siRNA negative control, CON: DMSO-treated.

Figure 7. The inverse correlation between PARP1 and PD-L1, PAR, and p-STAT3 expression in surgical specimens of ovarian cancer. **A**, Patient tissues were stained with PARP1 and PD-L1. Representative images of IHC staining of PARP1 and PD-L1 in human ovarian cancer tissues (n=41) are shown. Scale bar: 100 μ m. The correlation analysis between PARP1 and PD-L1 was analyzed, and the *P* value was calculated by the Pearson correlation test. ($P=0.0002$, $r= -0.54784$). ‘-’, negative expression; ‘+’, low expression; ‘++’, medium expression; ‘+++’, high positive expression. **B**, Patient tissues were stained with anti-PAR and anti-p-STAT3. Representative images of IHC staining of PAR and p-STAT3 in human ovarian cancer tissues (n=53) are shown. Scale bar: 100 μ m. ($P<0.0001$, $r= -0.8953$). **C**, PARP1-mediated poly(ADP-ribosyl)ation of STAT3 as a key

step in inhibiting the transcription of PD-L1. A graphical description of how PARP1 suppresses the transcription of PD-L1 by poly(ADP-ribosyl)ating STAT3.

Figure 1

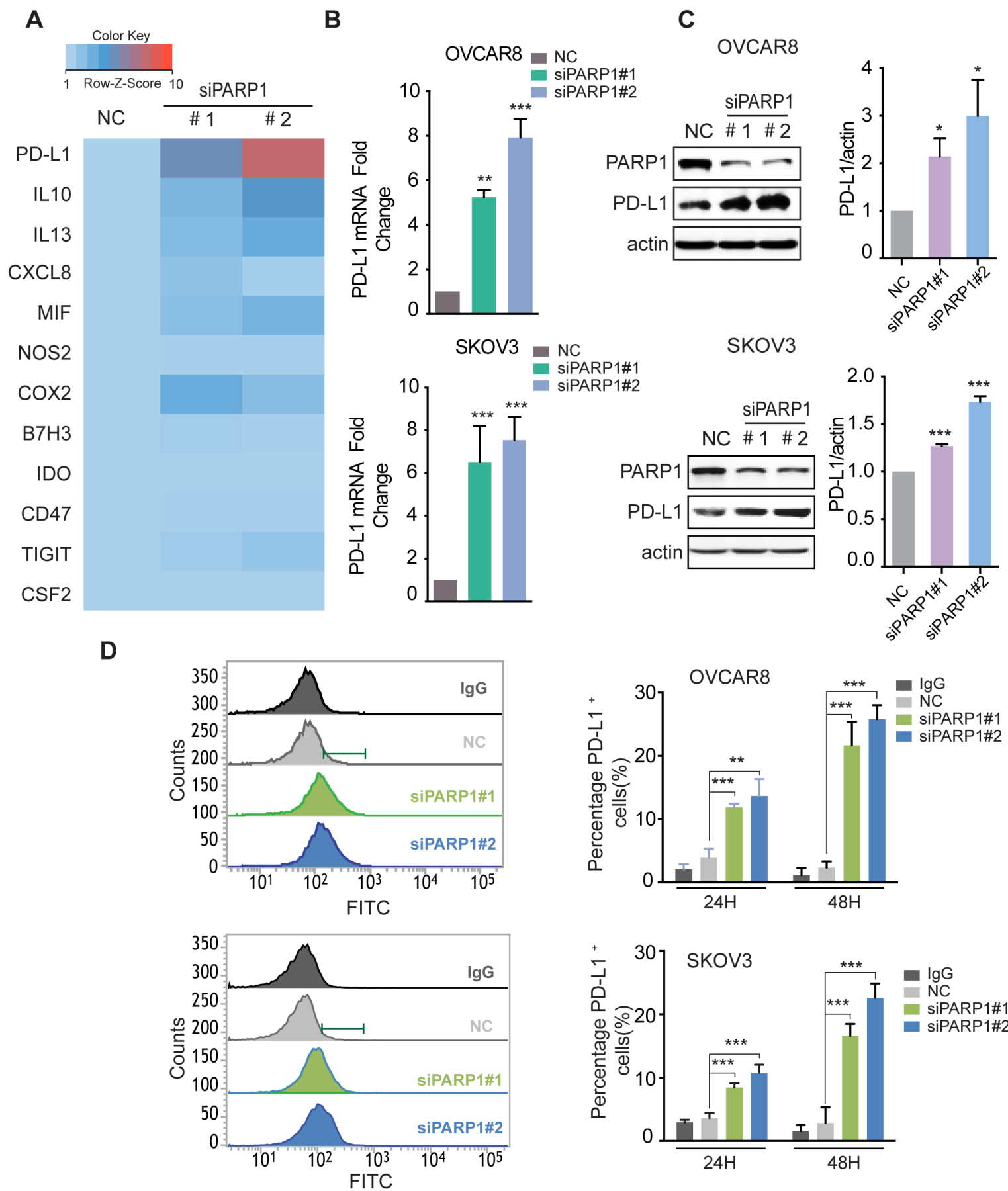


Figure 2

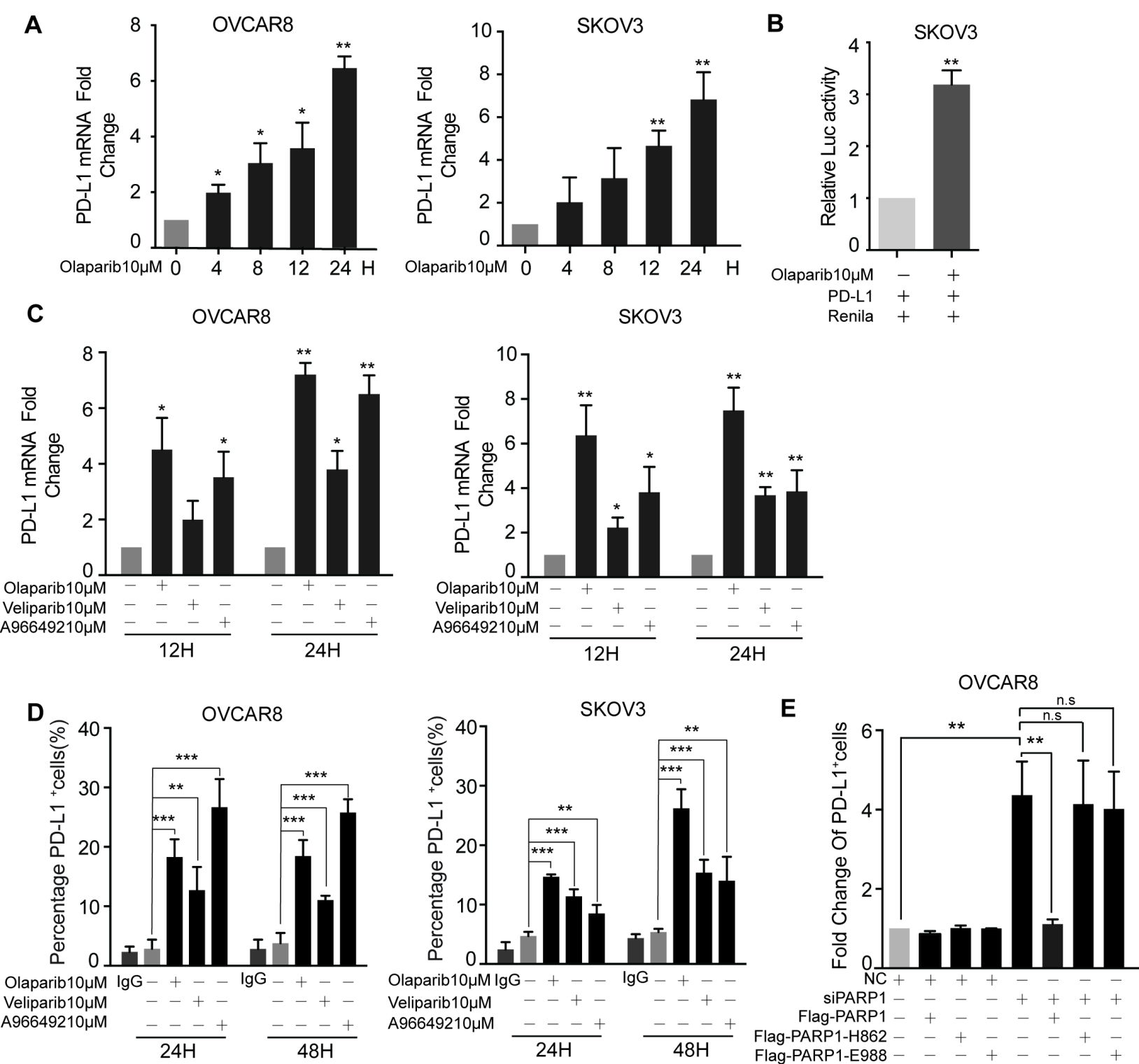
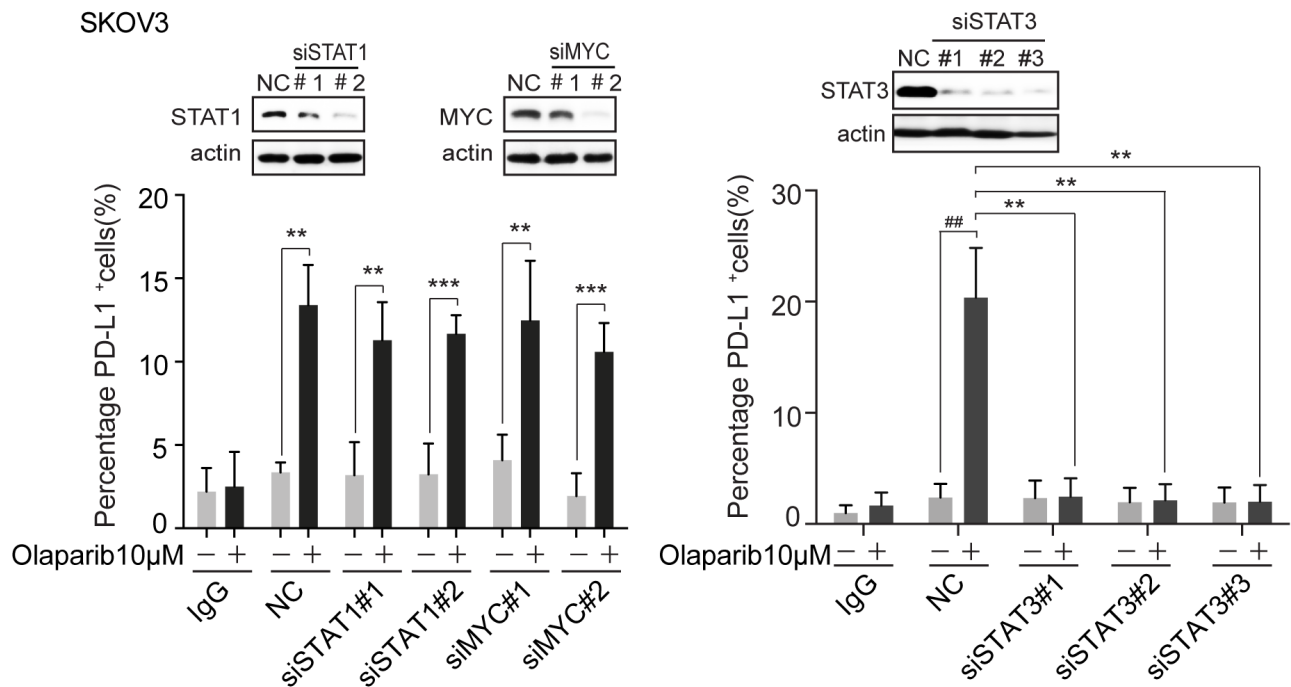
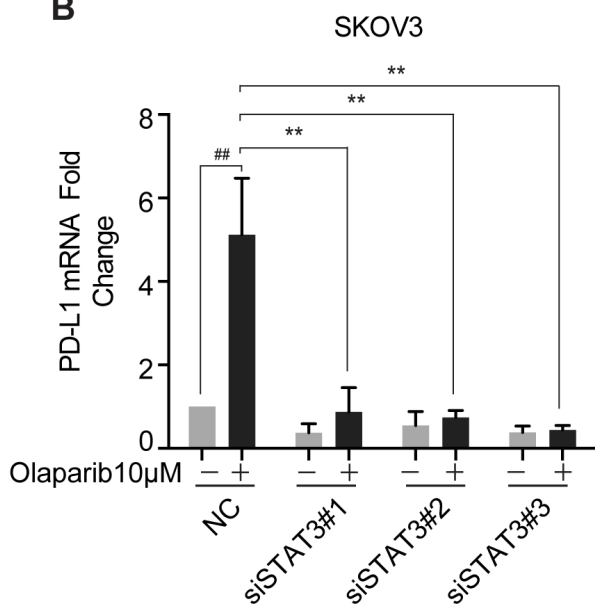


Figure 3

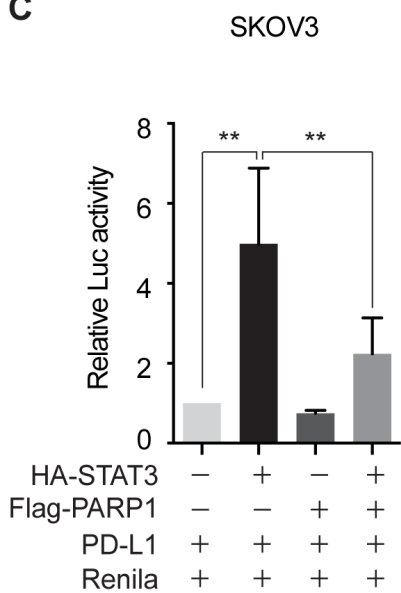
A



B



C



D

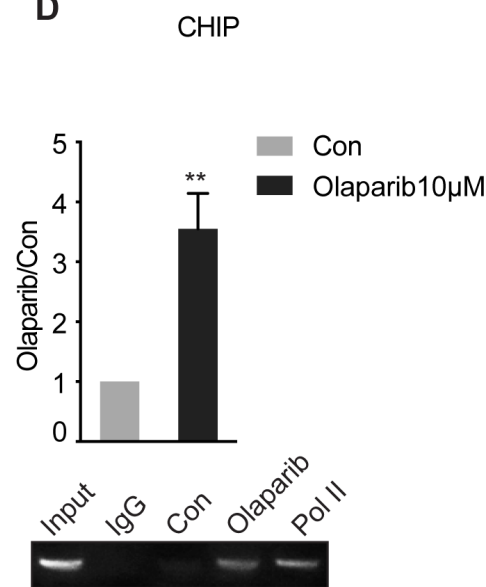


Figure 4

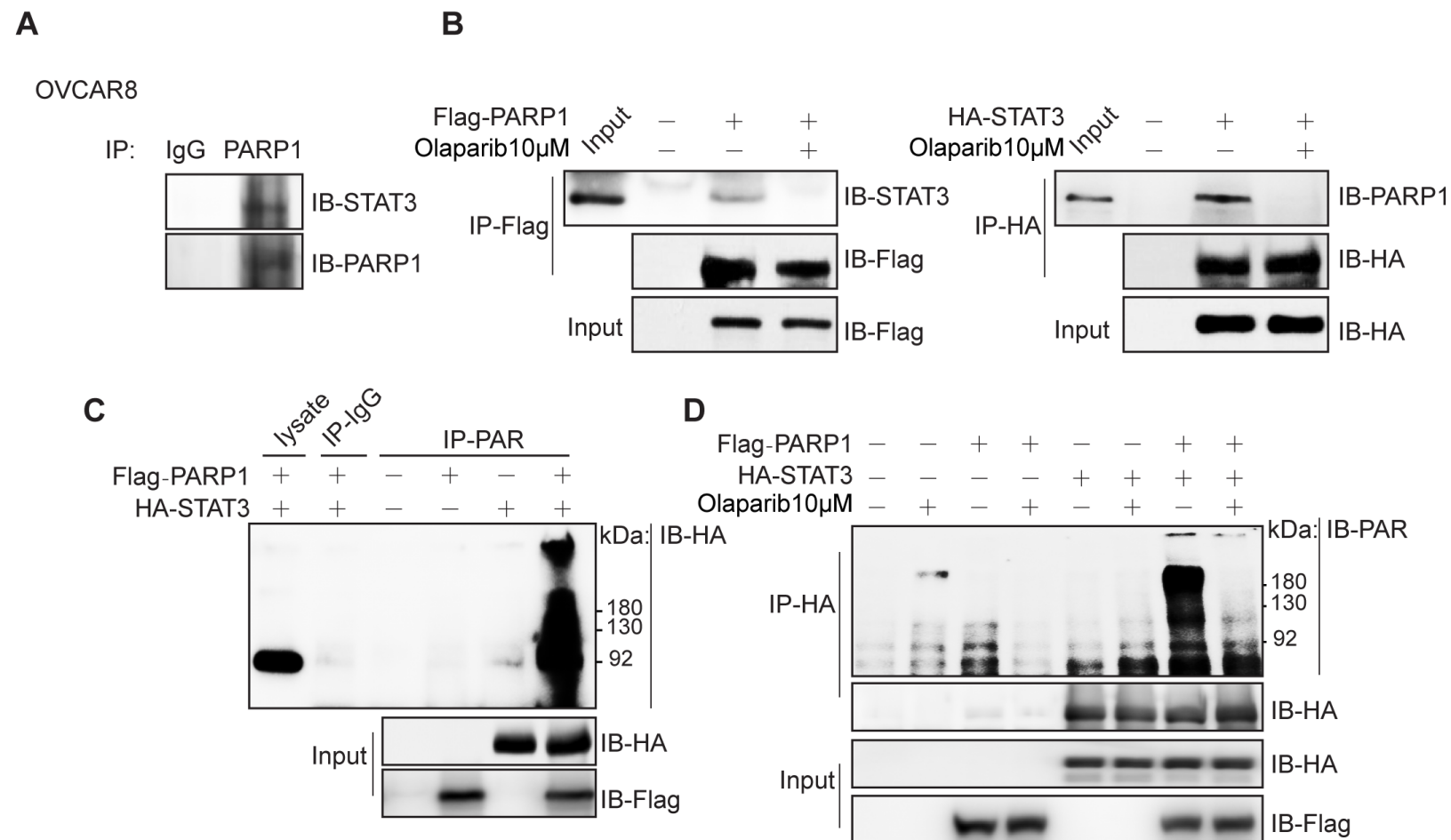


Figure 5

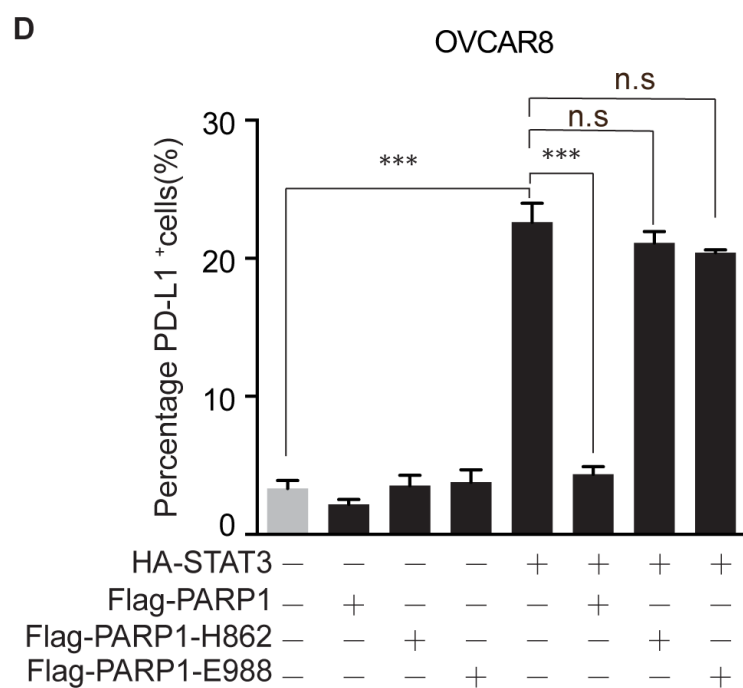
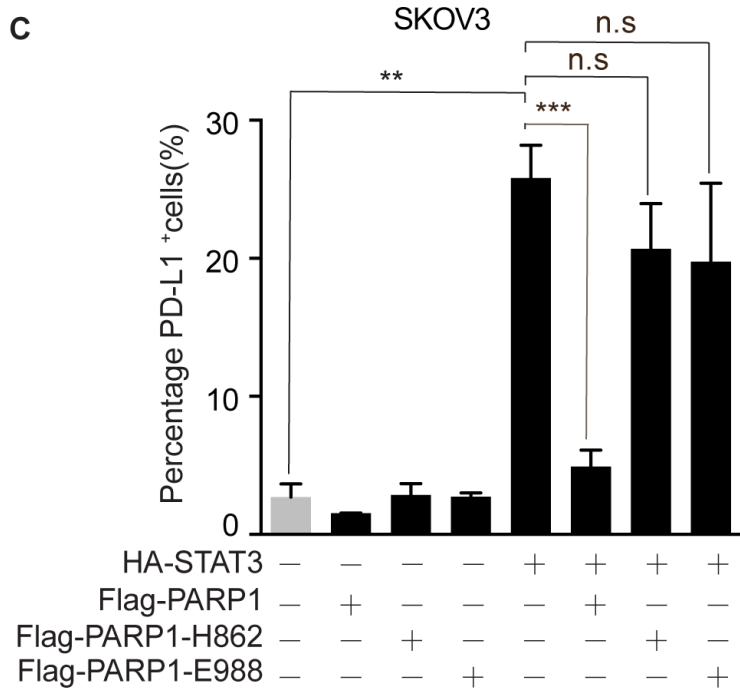
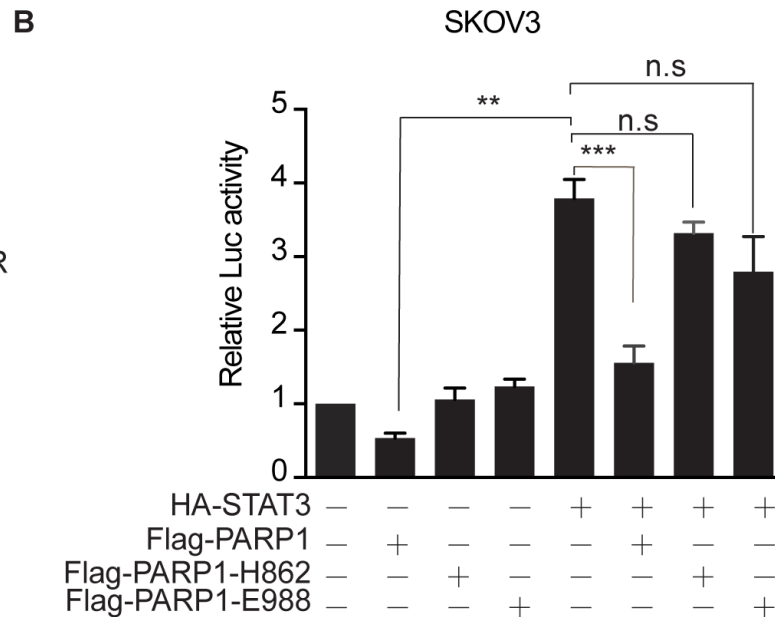
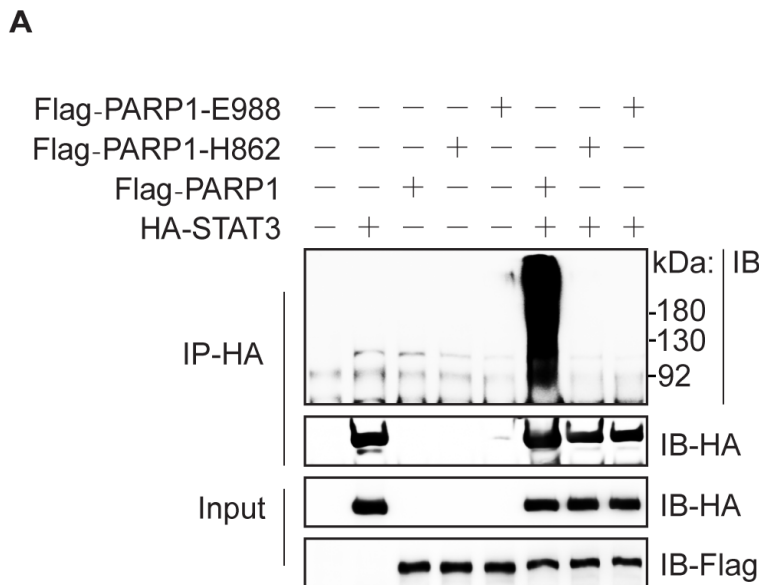


Figure 6

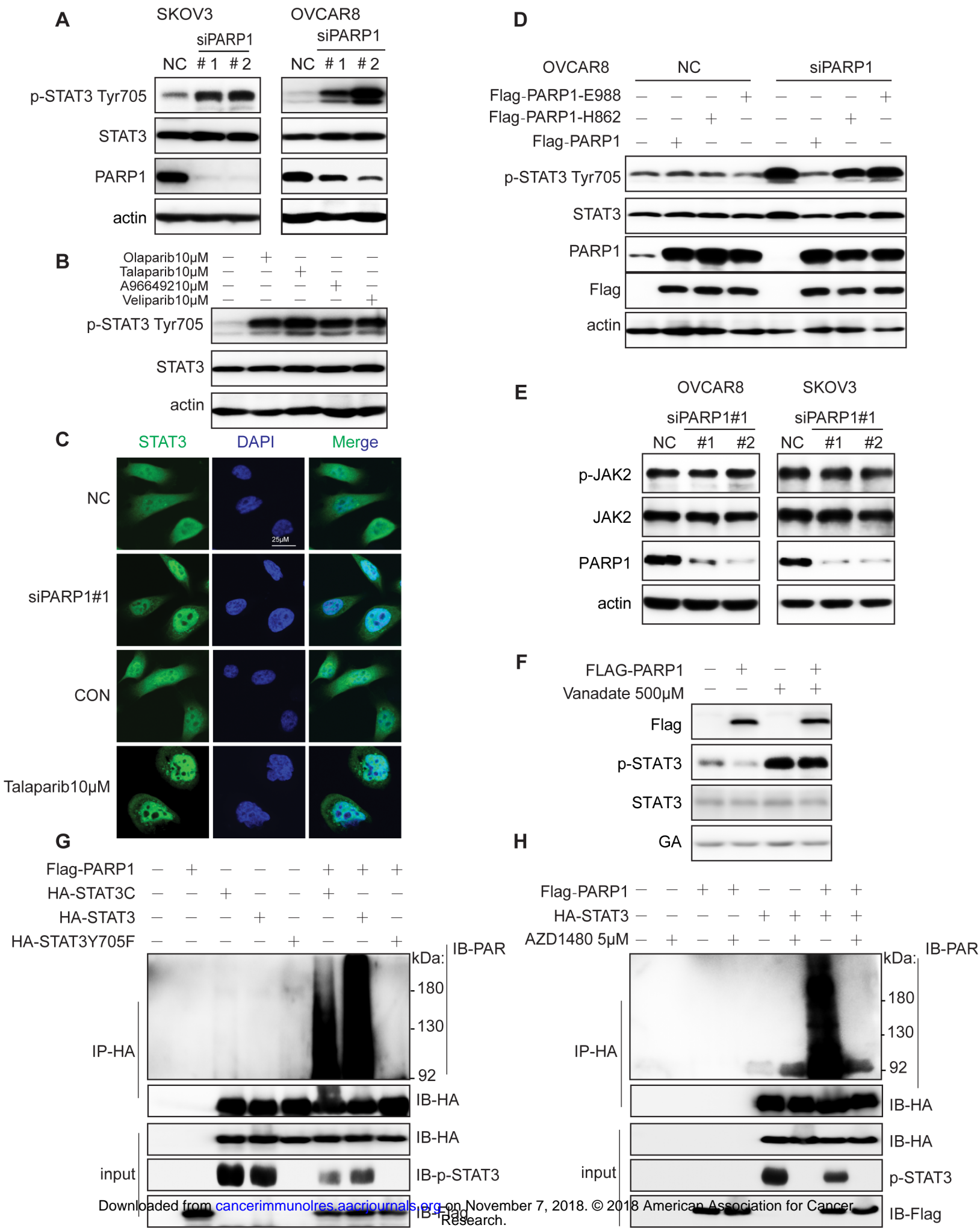
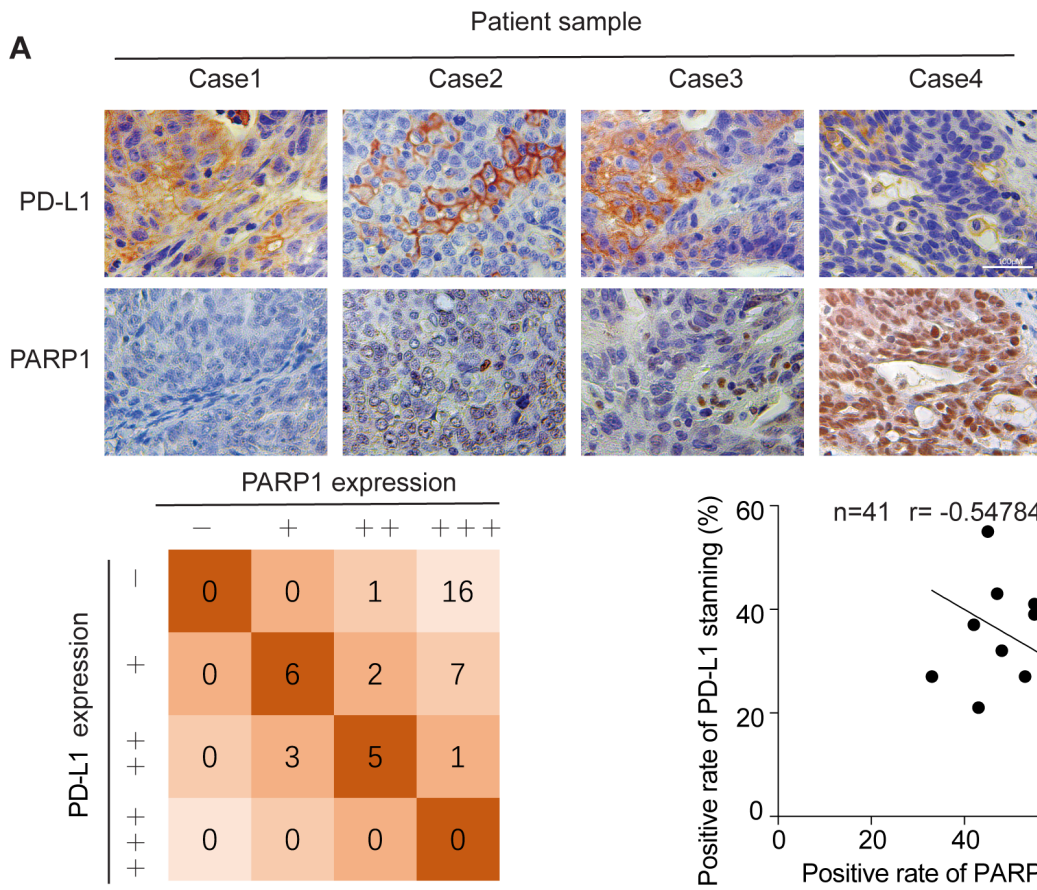
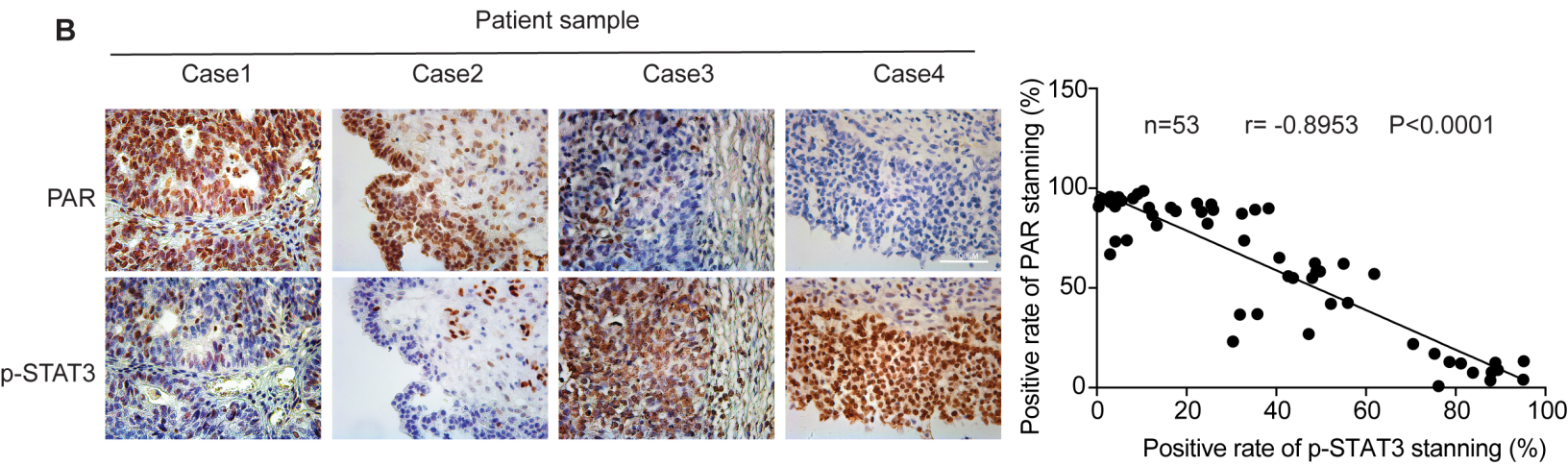


Figure 7

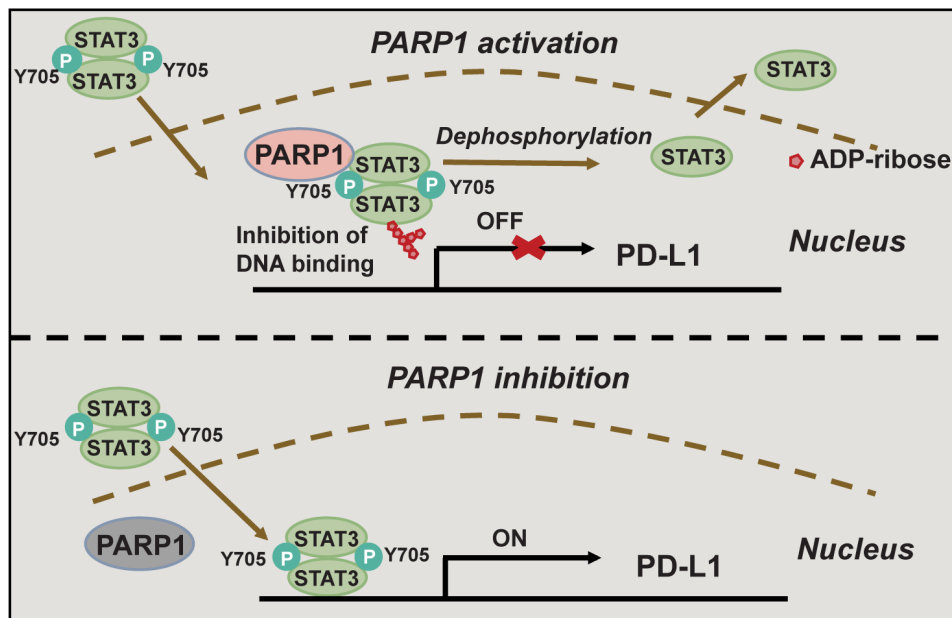
A



B



C



Cancer Immunology Research

PARP1 Suppresses the Transcription of PD-L1 by Poly(ADP-Ribosyl)ating STAT3

Ling Ding, Xi Chen, Xiaqing Xu, et al.

Cancer Immunol Res Published OnlineFirst November 6, 2018.

Updated version	Access the most recent version of this article at: doi: 10.1158/2326-6066.CIR-18-0071
Supplementary Material	Access the most recent supplemental material at: http://cancerimmunolres.aacrjournals.org/content/suppl/2018/11/06/2326-6066.CIR-18-0071.DC1
Author Manuscript	Author manuscripts have been peer reviewed and accepted for publication but have not yet been edited.

E-mail alerts	Sign up to receive free email-alerts related to this article or journal.
Reprints and Subscriptions	To order reprints of this article or to subscribe to the journal, contact the AACR Publications Department at pubs@aacr.org .
Permissions	To request permission to re-use all or part of this article, use this link http://cancerimmunolres.aacrjournals.org/content/early/2018/11/06/2326-6066.CIR-18-0071 . Click on "Request Permissions" which will take you to the Copyright Clearance Center's (CCC) Rightslink site.